Hierarchical Superhydrophobic Surfaces Resist Water Droplet Impact

Kripa K. Varanasi[*,1], Tao Deng[**,2], Ming Hsu[**], Nitin Bhate[**]
[*]Massachusetts Institute of Technology, Cambridge, MA
[**]GE Global Research Center, Niskayuna, NY

ABSTRACT

In this paper, we present static and dynamic wetting interactions of water droplets on a variety of superhydrophobic surfaces. For sessile droplets, wetting states were determined by measuring contact angles and comparing them to that obtained from equilibrium Cassie and Wenzel states. Surprisingly, we find that roll-off angles are minimized on surfaces expected to induce Wenzel-like wetting in equilibrium. We argue that droplets on these surfaces are metastable Cassie droplets whose internal Laplace pressure is insufficient to overcome the capillary pressure resulting from the energy barrier required to completely wet the posts. In the case of impacting droplets the water hammer and Bernoulli pressures must be compared with the capillary pressure. Experiments with impacting droplets using a high-speed camera and specific surface textures that can delineate various wetting regimes show very good agreement with this simple pressure-balance model. These studies show that hierarchical micro-nano surfaces are optimum for droplet impact resistance.

Keywords: superhydrophobic surfaces, droplet impact, wetting, hierarchical surfaces

1 INTRODUCTION

Droplet impingement on surfaces is a ubiquitous phenomenon in many industrial applications. In applications such as raindrops impacting a windshield, ice formation in aircraft engines and wind turbines, moisture-related erosion in power turbines, etc, there is substantial advantage to engineer surfaces with anti-wetting properties. Over the last decade there has been significant interest in the anti-wetting properties of lotus-leaf-inspired superhydrophobic surfaces[1]. Researchers have fabricated textured, hydrophobic surfaces through a range of methods to attain low roll-off angles. Methods include electrodeposition[2], nanotube growth[3], lithography[4], and wet etching[5]. Most of these studies characterized the wetting behavior of these surfaces using sessile droplet techniques and did not explore the dynamic interaction that occurs during the impact process. In this paper, we study both the static and dynamic interactions of droplets with a variety of superhydrophobic surfaces. Interactions with sessile droplets are quantified in terms of contact and roll-off angle while dynamic interactions with impacting droplets are observed using a high-speed camera. We find that effective contact angle, though a useful measure of the extent of hydrophobicity cannot be used to predict the droplet-impact resistance of these textured hydrophobic surfaces and the effect of dynamic pressures should be taken into account.

2 SESSILE DROPLETS

To understand the interactions of sessile droplets with these surfaces, we measure contact and roll-off angles on a series of post arrays where the post spacing (denoted by *b* in Figure 1) is systematically varied. To determine the droplet wetting state, we measure contact angle and compare results to predicted Cassie[6] and Wenzel[7] angles. For arrays of posts that are 15μm wide and 25μm high, an optimal post spacing region exists for droplet roll-off. Measurements are plotted in Figure 2 as a function of post spacing-to-width ratio *b/a*. For *b/a* ratio smaller than 1, 1μL droplets do not roll off, as indicated by values of 90°. When the *b/a* ratio is about 1.5, droplets begin to roll off, reaching minimum roll-off angles of about 17° at a *b/a* ratio of 5. However, for *b/a* ratio greater than about 6, droplets do not roll off.

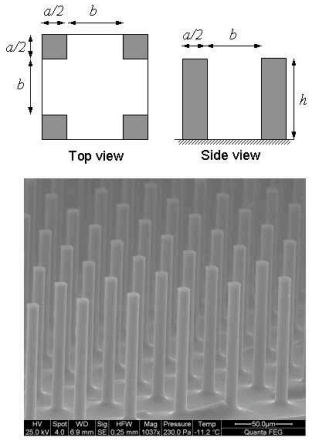

Figure 1: Schematic and SEM image of a representative post array. Top and side views of a unit cell illustrate definitions of post width *a*, spacing *b*, and height *h*.

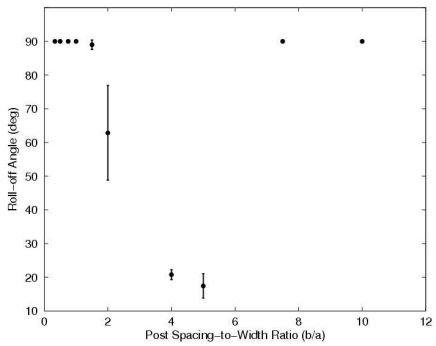

[1] Corresponding Authors: 1.Prof. Kripa K. Varanasi varanasi@mit.edu, 2. Dr. Tao Deng dengt@research.ge.com

Figure 2: Dependence of roll-off angle of 1μL water droplets on the *b/a* ratio of square posts that are 15μm wide and 25μm high.

To gain insight into droplet wetting state, we first calculate equilibrium contact angles according to the Wenzel and Cassie models. We then measure the contact angle of droplets on each texture and compare results with theory. Predictions and measurements for arrays of posts are plotted as a function of post spacing-to-width ratio *b/a* in Figure 3. Predicted contact angles for equilibrium Wenzel wetting (dashed line) fall from 180° at *b/a* of about 1.5 to about 122° at *b/a* of 10 while equilibrium Cassie angles (solid line) rise from about 135° to 175° for *b/a* ratios of 0.33 and 10, respectively. Because Cassie and Wenzel curves cross at *b/a* of about 1.8, energy minimization should favor Cassie wetting for *b/a* smaller than 1.8 and Wenzel wetting for *b/a* greater than 1.8.[8] Indeed, measured contact angles (solid circles) are consistent with Cassie wetting for *b/a* ratios that are less than about 2 and with Wenzel wetting for *b/a* ratios that are greater than 6. However, in the intermediate spacing regime, measured angles do not agree with either equilibrium wetting state. Droplets in this intermediate state exhibit optimum roll-off behavior and permit direct light transmission between droplet and surface (left image) as opposed to Wenzel droplets (right image), evidence that this intermediate state is Cassie-like.

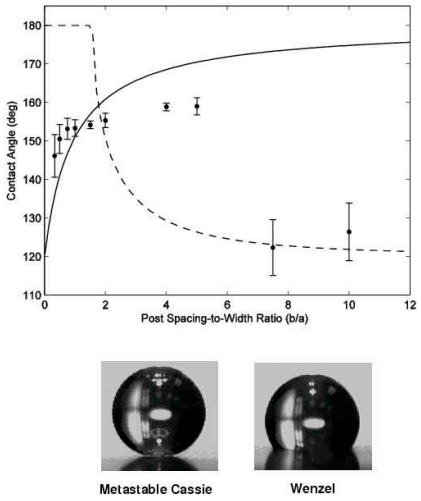

Figure 3: Dependence of static contact angle of 1μL water droplets on the *b/a* ratio of square posts that are 15μm wide and 25μm high. Solid and dotted lines denote values predicted for Cassie and Wenzel wetting states, respectively, while solid circles represent measurements.

Persistence of Cassie-like droplets in the equilibrium Wenzel regime indicates that there is an energy barrier[9-12] that maintains the droplet in a metastable state and prevents water from infiltrating into the texture. Hydrophobic materials will resist wetting because there is an associated energy cost. As the air-water interface penetrates deeper into the structures and the water wets a greater solid surface area, the total interfacial energy increases. An effective force required to wet these surfaces can be calculated by differentiating the energy with respect to the penetration depth. Normalizing by the air-water interfacial area yields the required pressure to force water into the texture, or capillary pressure P_C. For a square array of square posts of width *a* and edge-to-edge spacing *b*, the capillary pressure is given by

$$P_C = \left(\frac{-4\cos\theta_0}{\left(1 + b/a\right) - 1} \right) \frac{\gamma_{LV}}{a} \qquad (1)$$

where γ_{LV} is the air-water surface energy. Hydrophobic materials have values of θ_0 that exceed 90°, resulting in positive values of P_C corresponding to pressures that resist water penetration. Conversely, textures of hydrophilic materials (θ_0 < 90°) have negative P_C values, consistent with the tendency of hydrophilic capillaries to draw water in. For water and air, γ_{LV} = 0.072 J/m^2. Because our model surfaces are periodic with well-defined posts, given the intrinsic surface energy of a smooth surface of the same composition, we can then calculate capillary pressures exactly for each texture.

Wetting state is determined not only by the energy level of each state, but also the accessibility of each state. Because our droplets are placed on top of the textures and thus begin in a Cassie-like state, the energy landscape between this initial state and the lowest energy state will determine whether droplets can minimize total interfacial energy. The slope of the energy barrier is proportional to the capillary pressure, which will resist wetting and thus impede Cassie-to-Wenzel transitions. Capillary pressure decreases as the post spacing increases because there are fewer posts to wet per unit area. In the absence of external impulses, Laplace pressure $P_L = 2\gamma_{LV}/R$ where *R* is the droplet radius, is the driving force that facilitates wetting transitions. At a critical spacing-to-width ratio of about 5.5, the capillary pressure for 15μm posts equals the Laplace pressure. At larger values of post spacing, we expect Laplace pressure to overcome capillary pressure and allow droplets to transition to their equilibrium Wenzel state. This prediction is in agreement with the contact angle measurements of Figure 3 in which contact angles transition to predicted Wenzel values beyond the critical post spacing. The above prediction is further validated by the roll-off angle measurements of Figure 2 in which droplet roll-off angles decrease with spacing and reach minimum values on surfaces with spacing ratios that are slightly narrower than the critical spacing ratio. This is because droplets on these surfaces exist in Cassie state (ranging from equilibrium to metastable states) and therefore experience continuous reduction in contact-line pinning as the spacing ratio is increased. However, beyond the critical spacing, droplets do not roll-off as they transition into the Wenzel state and experience substantial increase in contact-line pinning. Therefore, this simple pressure balance model can predict whether surfaces will enable metastable wetting and optimal roll-off performance or equilibrium Wenzel wetting and poor roll-off characteristics.

Because pressures that force fluid into textures are not limited to Laplace pressures, it is desirable to design textures with higher capillary pressures to resist homogeneous wetting. For example, moving droplets exert dynamic pressures that can far exceed Laplace pressures. As given in (1), simply scaling down the feature size increases capillary pressure. For an array of square posts capillary pressure does not depend on feature height. However, shrinking in the lateral dimensions increases the capillary pressure because the differential vertical surface area of posts increases. For example, shrinking a post array by a factor of two is equivalent to cutting each post into four smaller posts, effectively doubling the differential vertical surface area.

3 IMPACTING DROPLETS

To design superhydrophobic surfaces for application onto products such as windshields or aircraft engines, one must consider the effect of impinging water droplets. These droplets can travel at elevated velocities and exert high pressures onto surfaces upon impact. To ensure that superhydrophobic surfaces maintain functionality in specific applications, it is crucial to prevent water infiltration into textures. This requires the texture-dependent capillary pressure (1) to exceed the droplet impact pressures. At the instant of impact a shock wave is set up in the droplet, giving rise to the so-called water hammer pressure[13]

$$P_{WH} = 0.2\rho CV \tag{8}$$

where ρ is the density of the liquid, C is the speed of sound in the liquid, and V is the velocity of the droplet. After the instant of impact the wetting pressures drop to the familiar Bernoulli pressure given by

$$P_B = \rho V^2/2 \tag{9}$$

This sequence of events is schematically shown in Figure 4.

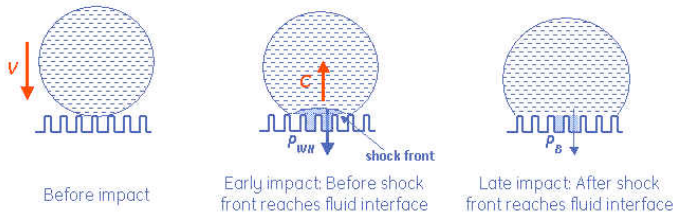

Figure 4: Sequence of droplet impact on superhydrophobic surfaces

The water hammer pressure is significantly higher than the Bernoulli pressure. For example, for a droplet impinging on a surface at 3m/s the water hammer pressure is around 0.9 Mpa when compared to a Bernoulli pressure of about 4.5 kPa. To facilitate complete droplet recoil and prevent droplet infiltration the surface texture of the superhydrophobic surface should be designed such that the capillary pressure P_C exceeds both the water hammer and Bernoulli pressures. When the capillary pressure is smaller than Bernoulli and water hammer pressures the droplet infiltrates the texture and remains pinned to the surface. However when the capillary pressure is greater than Bernoulli pressure but lower than the water hammer pressure partial pinning of the droplet should occur. These conditions are summarized in the following equations

$$\begin{aligned} &P_C < P_B < P_{WH} \text{ – complete infiltration and pinning} \\ &P_B < P_C < P_{WH} \text{ – partial pinning} \\ &P_B < P_{WH} < P_C \text{ – complete recoil} \end{aligned} \tag{10}$$

To validate our model, we conduct several droplet impact experiments with droplets impinging a surface with a velocity V~3m/s and capture the impact phenomenon on a high-speed camera. The texture parameters such as feature size, spacing, and aspect ratio are systematically varied. Here, we present results of droplet impact on four different surfaces to validate our pressure balance model. These surfaces are: 15 micron posts with edge-to-edge spacing of 150 microns, 15 microns posts with edge-to-edge spacing of 5 microns, nano-porous surface with pore diameter of 90 nm and center-to-center spacing of 100 nm, and a hierarchical surface with nanodendrites (~100nm) on microposts (3microns). The capillary pressures for these surfaces can be calculated to be 80 Pa, 12 kPa, and 1.6 MPa, and 0.92 MPa respectively. The photographs of the impact event are shown in Figure 5 along with the SEM images of the different surfaces. These results are in excellent agreement with our predictions.

4 CONCLUSIONS

We demonstrate that metastable Cassie droplets have superior roll-off properties when compared to equilibrium Cassie and Wenzel droplets. By systematically increasing the spacing between posts, we show that droplet wetting regime transitions from equilibrium Cassie to metastable Cassie and finally to equilibrium Wenzel regime. We propose a simple pressure balance model that predicts the transition from metastable Cassie to equilibrium Wenzel wetting. Measurements on textured hydrophobic surfaces with varying post spacing and size show good agreement with the model. In many cases, the metastable regime occupies a significant region of design space and we show that this additional design space can be utilized. We demonstrate that this trade-off can be circumvented by the use of smaller feature sizes. Our analysis and experiments show that similar textures with smaller feature length scales offer more capillary pressure to resist wetting. This further extends the metastable regime and provides an additional barrier against droplets that wet with greater pressures, such as falling raindrops and water droplets impacting moving surfaces. Smaller textures also offer a geometric advantage, as they restrict the size of droplets that can fit in between the textures. For example, droplets encountered during flight in aircraft engine applications can move as fast as 60m/s relative to the aircraft and are often smaller than 20μm in diameter. In this important application, wetting dynamics and freezing kinetics are also of concern. Nevertheless, our work validates a simple picture based on pressure balance that provides a framework for the predictive design of surfaces with optimal water-repellant and droplet shedding properties for many applications (such as dropwise condensation[14], deicing[15], etc.).

Figure 5: Dynamic interactions of 1mm diameter droplets with a variety of surfaces captured using a high-speed camera (a) Microtextured surface consisting of 15um posts spaced apart by 150um – droplet does not recoil (b) Partial recoil on microtextured surface consisting of 15um posts spaced apart by 5um (c) Hierarchical texture comprising of 3um posts with 100nm dendritic structures causes complete recoil and shedding (c) Metaloxide nanoporus surface with 90 nm pores results in complete drop recoil and shedding.

ACKNOWLEDGEMENTS

We thank Dr. Margaret Blohm and the Nanotechnology Program at GE Global Research Center for support.

References

[1] Barthlott, W.; Neinhuis, C. *Planta* **1997**, 202,

[2] Shirtcliffe, N.J.; McHale, G; Newton, M.I.; Perry, C.C. *Langmuir* **2005,** 21, 937.

[3] Lau, K.K.S.; Bico, J; Teo, K.B.K.; Chhowalla, M.; Amaratunga, G.A.J.; Milne, W.I.; McKinley, G.H.; Gleason, K.K. *Nano Lett.* **2003** 3, 1701.

[4] Oner, D; McCarthy, T.J. *Langmuir* **2000** 16, 7777.

[5] Guo, Z; Zhou, F; Hao, J; Liu, W. *J. Am. Chem. Soc.* **2005** 127, 15670.

[6] Cassie, A.B.D.; Baxter, S. *Trans. Faraday Soc.* **1944** 40, 546.

[7] Wenzel, R.N. *Ind. Eng. Chem.* **1936** 28, 988.

[8] Patankar, N.A. *Langmuir* **2003** 19, 1249.

[9] Marmur, A. *Langmuir* **2004** 20, 3517.

[10] L Barbieri, E Wagner, and P Hoffmann, Langmuir **23**, 1723 (2007).

[11] Lafuma, A.; Quéré, D. *Nature Mater.* **2003** 2, 457

[12] Tuteja et.al., MRS Bulletin, 2008

[13] Huang et. al, *Journal of Fluids Engineering, Transactions of the ASME*, v 95 Ser I, n 2, Jun, 1973, p 276-294

[14] Varanasi, K.K.; Bhate, N. et.al., *US Patent Application* **2005** Application Number: 20070028588

[15] Hsu, M.F.; Varanasi, K.K., et.al., *US Patent Application* **2005** Application Number: 20070031639